Available online at www.sciencedirect.com

SCIENCE DIRECT

Journal of Sound and Vibration 274 (2004) 777–799

JOURNAL OF SOUND AND VIBRATION

www.elsevier.com/locate/jsvi

# In-plane free vibration analysis of circular arches with varying cross-sections using differential quadrature method

G. Karami[a,]*, P. Malekzadeh[b]

[a] Department of Mechanical Engineering and Applied Mechanics, North Dakota State University, Fargo, ND 58105, USA

[b] Department of Mechanical Engineering, School of Engineering, Persian Gulf University, Busher 75168, Iran

Received 16 July 2002; accepted 15 June 2003

**Abstract**

A differential quadrature (DQ) methodology recently developed by the authors is used to obtain a general and a computationally efficient and accurate DQ solution for free vibration of variable cross-section circular thin arches. As an improvement to the classical theory and in order to evaluate the higher order natural frequencies more accurately, the commonly used hypothesis of "the inextensibility of the central axis" is removed. This enables one to study the effects of slenderness ratio on the natural frequencies, especially at higher order modes. Rotary inertia is included in the formulation and its influence on natural frequencies is studied. Arches with different types of boundary conditions, including those with elastic constraint against rotation at their ends, are considered. For the cases where a change in the cross-sectional or material properties of the arch occurs, a numerical domain decomposition technique in conjunction with DQ methodology is developed and incorporated. To verify the accuracy of the methodology, the results are compared with those of exact solutions and/or other approaches such as finite elements, Rayleigh–Ritz, Galerkin, cell discretization methods, and other DQ methodologies. In particular, excellent solution agreements are achieved with those of exact solutions, the generalized differential quadrature rule and the optimized Rayleigh–Ritz method solutions.



## 1. Introduction

Due to practical importance of circular arches, many researchers have studied static as well dynamic behavior of such elements. The numerical simulations are mostly based on finite elements, Rayleigh–Ritz, Galerkin, and cell discretization methods. A review on the different methods of analysis for circular arches has been recently presented by Auciello and De Rosa [1].

*Corresponding author.

*E-mail address:* G.Karami@ndsu.nodak.edu (G. Karami).

0022-460X/$ - see front matter © 2003 Elsevier Ltd. All rights reserved.
doi:10.1016/S0022-460X(03)00786-7

Tong et al. [2] have used the exact solution of inextensible thin uniform circular arches to study the in-plane free and forced vibration of circular arches with stepped cross-sections. As a consequence, they have used their method to obtain an approximate solution for arches with non-uniform cross-sections.

Basically, the governing equations of the thin arches include fourth and second order partial differential equations (PDEs). In most studies in order to simplify the system of equations, an additional assumption of the inextensibility (or incompressibility) of the centroidal axes has been employed. Using this assumption, the two-coupled partial differential governing equations are reduced to a sixth order partial differential equation. However, in order to improve the accuracy of natural frequency evaluations, especially at higher order modes, it is suggested that axial deformation should be accounted for [3,4]. As an alternative simplifying assumption for inextensible arches, one may neglect the effect of tangential inertias [5,6]. This approach which is called "approximate theory" after De Rosa and Franciosi [6] may be employed only for shallow arches in conjunction with the inextensible centroidal axes assumption [5,6].

In this paper, a DQ method is used to solve the basic governing equations of thin circular arches comprising both radial as well as tangential displacements as field variables. The slenderness ratio as a design parameter would thus be introduced in the governing equations. Arbitrary variable cross-section arches with a system of PDEs having variable coefficients are considered. Closed form solutions to such a system of PDEs do not exist. The efforts here are focused to develop a DQ solution for such a system of equations to reduce the amount of computations, and also to provide a general and simpler numerical DQ scheme. It is a known fact that the difficulty in implementing multiple boundary conditions of a field variable is a draw back in conventional DQ methods [7]. Here, a recently developed DQ methodology [8,9] is to be employed to implement the multiple boundary conditions at boundary points in a more efficient manner. The applicability of this DQ methodology has been tested for beam elements [8] and for rectangular plates of any classical and some non-classical boundary conditions, such as a plate with point supports [9]. Excellent results have been achieved for all cases, and especially for those cases that conventional DQ methods have not yielded a converged solution or have resulted to low accuracy solutions. The efficiency of this methodology was further demonstrated in another application for the quadrilateral straight-sided plates [10]. The present study however differs from the previous studies due to the fact that here, unlike in previous cases, a system of equations constructed from second and fourth order PDEs with variable coefficients have to be solved. In the ongoing study, any type of classical boundary conditions for arches is to be considered. In addition, non-classical boundary condition type of elastically restrained against rotation would also be incorporated. To account for any changes in geometrical and/or material properties a special domain decomposition technique is developed. Examples are solved to verify the implementation. To verify the accuracy, the results for extensible and inextensible arches and also the results based on the approximate theory are compared with those of exact and other methods and in special cases with other DQ methods.

In DQM applications to arches, Gutierrez and Laura [11] have used DQ in conjunction with the $\delta$-technique to obtain the fundamental natural frequency of continuously variable section ring type arches. They have used inextensible theory to investigate simply supported and completely free arches. Kang et al. [12] have also used the same procedure to study both extensible and inextensible uniform cross-sectional circular arches. They have obtained the fundamental natural frequencies for arches with simply supported and clamped boundary conditions. Using the same method, the effects of warping have been considered in another effort by Kang et al. [13]. Kang and co-workers have also considered the free vibration of shear deformable arches [14]. De Rosa and Franciosi [6] have used a DQ method to study inextensible, uniform circular arches with clamped, simply supported and clamped–free boundary conditions. More recently Liu and Wu [15] have used the generalized differential quadrature rule to study the free vibration of inextensible circular arches. Variable cross-section arches under different types of classical boundary conditions have been examined. They have reported the natural frequencies up to only the second mode.

One point to be noted here is that by considering the governing equations of extensible arches, other DQ methods, which employ the first order derivative as a degree of freedom [6,15], require more effort for implementation of boundary conditions. This is because the weighting coefficients in such cases depend on the order of governing PDEs and one cannot use the weighting coefficients of fourth order PDEs for second order PDEs. Therefore, for the problem under consideration, one should evaluate two sets of weighting coefficients, which increases the computational effort. In the analysis, the generalized differential quadrature rule (GDQR) is used as a computationally efficient technique for evaluation of weighting coefficients. It should be mentioned that Liew and Liu [16], Liew et al. [17] and Du et al. [18] have used GDQR for free vibration analysis of shear-deformable annular sector plates and cross-ply laminates, and also for the buckling analysis of classical beams and plates.

## 2. DQM formulations and implementations

### 2.1. Governing equations of arches

Consider a thin variable section arch as shown in Fig. 1. A material point on the centroidal axis of the undeformed arch is located by angle $\theta$ as shown in Fig. 1. The radius of curvature of the centroidal axis is denoted by $R$, the opening angle by $\theta_o$, and the radial and tangential displacements of a material point on the centroidal axis by $u$ and $w$, respectively.

Governing equations for such an arch, which include the effects of axial deformation and rotary inertia can be derived from the principle of total potential energy in a systematic

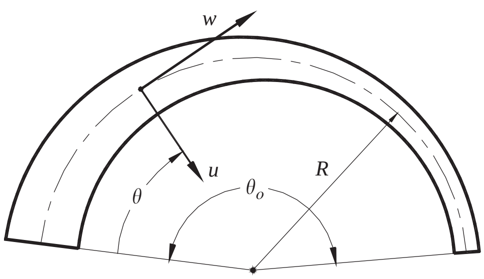


Fig. 1. Geometry of circular arch.

manner as

$$\frac{AE}{R^2}w'' + \frac{(AE)'}{R^2}w' - \frac{AE}{R}u' - \frac{(AE)'}{R}u + \rho R\omega^2\left[\left(A + \frac{I}{R^2}\right)w + \frac{I}{R^2}u'\right] = 0, \quad (1)$$

$$\left(\frac{EI}{R^3}\right)u'''' + \frac{2}{R^3}(EI)'u''' + \left[\frac{1}{R^3}(EI)'' + \frac{2EI}{R^3}\right]u'' + \frac{2}{R^3}(EI)'u'$$
$$+ \left[\frac{(EI)''}{R^3} + \frac{EI}{R^3} + \frac{EA}{R}\right]u - \left(\frac{EA}{R}\right)w' - \rho R\omega^2\left\{Au - \frac{1}{R^2}[I(w+u')]'\right\} = 0. \quad (2)$$

In the above equations each prime denotes one differentiation with respect to dimensionless coordinate variable $x$ ($= \theta/\theta_o$). The variables $R$, $A$ and $I$ are the curvature radius, cross-sectional area, and second area moment of inertia of the section of arch and $E$, $\rho$, $\omega$ are Young's modulus, density and natural frequency of the arch, respectively. In order to simplify the analysis, the following parameters are introduced:

$$A(x) = A_o a(x), \quad I(x) = I_o H(x), \quad S_r = R\theta_o/\kappa, \quad \kappa = \sqrt{I_o/A_o}, \quad \lambda^2 = \omega^2\left(\frac{\rho R^4}{EI_o}\right),$$

where $S_r$ represents the slenderness ratio of the arch, $\kappa$ is the radius of gyration and $\lambda$ and $\omega$ are the non-dimensional natural frequency and natural frequency, respectively. By introducing these parameters, one can rewrite governing equations (1) and (2) as

$$S_r^2(aw'' + a'w' - \theta_o a'u - \theta_o au') + \lambda^2\left\{\left[a + \left(\frac{\theta_o}{S_r}\right)^2 H\right]w + \left(\frac{\theta_o H}{S_r^2}\right)u'\right\} = 0, \quad (3)$$

$$Hu'''' + 2H'u''' + (H'' + 2H\theta_o^2)u'' + 2H'\theta_o^2u' + [\theta_o^2H'' + \theta_o^4H + (\theta_oS_r)^2a]u$$
$$- \theta_o aS_r^2w' + \lambda^2\left\{\frac{1}{S_r^2}[H'(\theta_o w + u') + H(\theta_o w' + u'')] - au\right\} = 0. \quad (4)$$

### 2.2. DQ analogues of governing equations

In order to construct the DQ analogues of the governing equations, one must define the degrees of freedom for the problem under consideration. For the present DQ methodology, the boundary degrees of freedom are displacements $(u, w)$ and the second derivative of the radial displacement $K$ ($= \mathrm{d}^2u/\mathrm{d}x^2$). Whereas on the interior domain, only the displacement components $(u, w)$ are chosen as degrees of freedom [8–10]. That is

$$\{U_b\} = [u_1 \;\; u_N \;\; w_1 \;\; w_N \;\; K_1 \;\; K_N]^{\mathrm{T}}, \quad \{U_d\} = [[u_2 \ldots u_{N-1}] \;\; [w_2 \ldots w_{N-1}]]^{\mathrm{T}}. \quad (5)$$

The subscripts $b$ and $d$ stand for boundary and interior domain degrees of freedom, respectively. Subscripts $1, 2, \ldots, N-1,\; N$ are grid point numbers. Thus, the grid points 1 and $N$ represent the grid at the ends of the arch where boundary conditions apply.

Two important factors that affect the accuracy of the DQ method are the accuracy of weighting coefficients and the choice of sampling points. Employing the present definitions for the degrees of freedom, no special treatments are needed to evaluate the weighting coefficients. This is not the case for other DQ methods such as those that employ the first order derivative as a field variable on the boundary. In the present analysis, an explicit algorithm is used. The algorithm is computationally efficient and yields the weighting coefficients most accurately, irrespective of the number and positions of sampling points [7]. In addition, there are no restrictions on the location of sampling points, and any grid generation rule for conventional DQ methods can be used for locating the sampling points. The description of how to evaluate the weighting coefficients is given in Appendix A.

Based on the choice of degrees of freedom the DQ analogues of the governing equations (3) and (4) becomes, respectively,

$$S_r^2\left(a_i\sum_{m=1}^{N}B_{im}w_m + a_i'\sum_{m=1}^{N}A_{im}w_m - \theta_o a_i' u_i - \theta_o a_i \sum_{m=1}^{N}A_{im}u_m\right) + \lambda^2\left\{\left[a_i + \left(\frac{\theta_o}{S_r}\right)^2 H_i\right]w_i + \left(\frac{\theta_o H_i}{S_r^2}\right)\sum_{m=1}^{N}A_{im}u_m\right\} = 0, \tag{6}$$

$$\begin{aligned} &H_i\sum_{n=1}^{N}\sum_{m=2}^{N-1}B_{im}B_{mn}u_n + 2H_i'\sum_{n=1}^{N}\sum_{m=2}^{N-1}A_{im}B_{mn}u_n + (2\theta_o^2 H_i + H_i'')\sum_{m=1}^{N}B_{im}u_m \\ &+ 2H_i'\theta_o^2\sum_{m=1}^{N}A_{im}u_m + [H_i\theta_o^4 + H_i''\theta_o^2 + (\theta_o S_r)^2 a_i]u_i + (H_iB_{i1} + 2H_i'A_{i1})K_1 \\ &+ (H_iB_{iN} + 2H_i'A_{iN})K_N - K_i(\theta_o^4)u_i - \theta_o S_r^2 a_i\sum_{m=1}^{N}A_{im}w_m \\ &+ \lambda^2\left\{\frac{1}{S_r^2}\left[H_i'\left(\theta_o w_i + \sum_{m=1}^{N}A_{im}u_m\right) + H_i\left(\theta_o\sum_{m=1}^{N}A_{im}w_m + \sum_{m=1}^{N}B_{im}u_m\right)\right] - a_iu_i\right\} = 0, \end{aligned} \tag{7}$$

for $i = 1, 2, \ldots, N$, where $N$ is the number of grid points. Eqs. (6) and (7) can be assembled in matrix form as

$$[[S_{db}] \quad [S_{dd}]]\left\{\begin{array}{c}\{U_b\}\\ \{U_d\}\end{array}\right\} - \lambda^2[[M_{db}] \quad [M_{dd}]]\left\{\begin{array}{c}\{U_b\}\\ \{U_d\}\end{array}\right\} = \{0\}. \tag{8}$$

Using the definition of boundary and domain degrees of freedom, i.e., Eq. (5), the elements of matrix coefficients in the above equation can be easily derived.

### 2.3. Boundary conditions

Some important types of boundary conditions that may be applied to a circular arch include the following.

#### 2.3.1. Elastically restrained against rotation (SR)

For this type of boundary condition the displacement components are fixed and the bending moment is balanced by bending moment produced by an elastic torsional spring at the support:

$$w = 0, \quad u = 0, \quad \frac{EI}{R}\frac{d^2u}{d\theta^2} + k_t n_b \frac{du}{d\theta} = 0, \tag{9}$$

where $n_b = -1$ for $\theta = 0$ and $n_b = 1$ for $\theta = \theta_o$; $k_t$ is the elastic coefficient of support.

*2.3.2. Clamped (C)*

$$w = 0, \quad u = 0, \quad \frac{du}{d\theta} = 0. \tag{10}$$

*2.3.3. Transversally guided support (G)*

An end with this type of boundary condition has fixed tangential and rotational degrees of freedom. The radial displacement has no constraint and therefore one has

$$w = 0, \quad \frac{du}{d\theta} = 0, \quad EI\left(\frac{d^3u}{d\theta^3} + \frac{d(EI)}{d\theta}\right)\left(\frac{d^2u}{d\theta^2} + u\right) = 0. \tag{11}$$

*2.3.4. Free end (F)*

Since no constraints are present for any movement at the arch ends, no reaction forces, i.e., axial force, shear force and bending moment, will be produced:

$$\frac{dw}{d\theta} - u = 0, \quad EI\left(\frac{d^3u}{d\theta^3} + \frac{du}{d\theta}\right) + \frac{d(EI)}{d\theta}\left(\frac{d^2u}{d\theta^2} + u\right) = 0, \quad \frac{d^2u}{d\theta^2} + u = 0. \tag{12}$$

*2.4. DQ analogues of boundary conditions*

Similar to the governing equations, the DQ analogues of the boundary conditions are developed.

*2.4.1. Zero displacement*

$$w_b = 0, \quad u_b = 0 \quad \text{for } b = 1 \text{ or } N. \tag{13}$$

*2.4.2. Zero slope*

The zero slope boundary conditions are implemented through the curvature as [8–10]

$$K_b - \sum_{n=1}^{N}\sum_{m=m_l}^{m_u} A_{bm}A_{mn}u_n = 0 \quad \text{for } b = 1 \text{ or } N, \tag{14}$$

where $m_l = 2$ if the end at $\theta = 0$ is clamped, otherwise it is equal to 1; also $m_u = N - 1$ if the end at $\theta = \theta_o$ is clamped, otherwise it is set to $N$.

*2.4.3. Bending moment*

The DQ analogues of a zero bending moment boundary condition and that which is balanced with the moment of an elastic spring at a boundary point, can be explained by an equation in the form of

$$H_b K_b + \theta_o^2 u_b + n_b \theta_o K_{bT} \sum_{m=1}^{N} A_{bm} u_m = 0 \quad \text{for } b = 1 \text{ or } N, \tag{15}$$

where $K_{bT} = k_{bt} R/(EI_o)$.

*2.4.4. Zero axial force*

$$\sum_{m=1}^{N} A_{bm} w_m - \theta_o u = 0 \quad \text{for } b = 1 \text{ or } N. \tag{16}$$

*2.4.5. Zero shear force*

$$H_b \left( \sum_{n=1}^{N} \sum_{m=2}^{N-1} A_{bm} B_{mn} u_n + \theta_o^2 \sum_{m=1}^{N} A_{bm} u_m \right) + H_b A_{b1} K_1 + H_b A_{bN} K_N + H_b' (K_b + \theta_o^2 u_b) = 0 \tag{17}$$

for $b = 1$ or $N$. The assembled form of the boundary conditions can also be represented in matrix form as

$$[S_{bb}]\{U\}_b + [S_{bd}]\{U\}_d = \{0\}. \tag{18}$$

Eliminating the boundary degrees of freedom from Eqs. (8) and (18) one has

$$[S]\{U_d\} - \lambda^2 [M]\{U_d\} = \{0\}, \tag{19}$$

where $[S] = [S_{dd}] - [S_{db}][S_{bb}]^{-1}[S_{bd}]$ and $[M] = [M_{dd}] - [M_{db}][S_{bb}]^{-1}[S_{bd}]$. From Eq. (19), one can obtain both the natural frequencies and the associated mode shapes.

## 3. The approximate theory

As an alternative to the previously developed general governing equations of thin arches, an "approximate theory," based on assuming negligible tangential inertias can be developed. After matrix partitioning of Eq. (19), the final system of equations for thin circular arches based on this approximate theory may be written as

$$\begin{bmatrix} [S_{uu}] & [S_{uw}] \\ [S_{wu}] & [S_{ww}] \end{bmatrix} \begin{Bmatrix} \{U_{du}\} \\ \{U_{dw}\} \end{Bmatrix} - \lambda^2 \begin{bmatrix} [M_{uu}] & 0 \\ 0 & 0 \end{bmatrix} \begin{Bmatrix} \{U_{du}\} \\ \{U_{dw}\} \end{Bmatrix} = \{0\}. \tag{20}$$

Using this equation, one can easily eliminate the tangential displacement components and obtain the simplified governing equation as

$$[\bar{S}]\{U_{du}\} - \lambda^2 [M_{uu}]\{U_{du}\} = \{0\}, \tag{21}$$

where $[\bar{S}] = [S_{uu}] - [S_{uw}][S_{ww}]^{-1}[S_{wu}]$. As one can expect, the slenderness ratio that appears in governing Eq. (21) should be taken very large ($S_r \geqslant 10^4$), since the formulation is based on extensible theory. Some examples for both shallow and deep arches are considered to prove the accuracy of this formulation.

## 4. Domain decomposition technique

When the coefficients in the governing partial differential equations suddenly change through the domain of interest, then domain decomposition becomes a necessity (see Fig. 2). For such problems, the vector of boundary degrees of freedom should be modified to include the displacements and the curvatures at the common sections of each two adjacent sub-domains. For example, consider the section '$i$' of the two sub-domains '$i$' and '$i+1$' in Fig. 2. The new boundary degrees of freedom at this common section are $[u_{ic} \;\; w_{ic} \;\; K_{iL} \;\; K_{iR}]$. Subscripts '$c$', '$L$' and '$R$' stand for common, left and right of a common section '$i$'. Therefore, the boundary degrees of freedom become

$$\begin{aligned}\{U_b\} = [&[u_1 \quad u_N] \quad [w_1 \quad w_N] \quad [K_1 \quad K_N] \quad [u_{1c} \quad w_{1c} \quad K_{1L} \quad K_{1R}] \\ &\ldots [u_{N_c c} \quad w_{N_c c} \quad K_{N_c L} \quad K_{N_c R}]]^{\mathrm{T}},\end{aligned} \tag{22}$$

where $N_c$ is the number of common sections of the individual sub-domains.

The governing equations of each sub-domain is similar to those of a single domain obtained in Sections 2.1 and 2.2. In addition to the external boundary conditions, the geometric and physical compatibility should be satisfied at the common sections of the two adjacent sub-domains. The geometric compatibility conditions include the continuity of tangential and radial displacements, and the slopes. The continuity of the displacement components is automatically satisfied, since they are chosen as the degrees of freedom. The continuity of slope at the interface of sub-domains '$i$' and '$i+1$' is written as

$$\left(\frac{\mathrm{d}u}{\mathrm{d}\theta} + \frac{w}{R}\right)\Bigg|^{(i)} - \left(\frac{\mathrm{d}u}{\mathrm{d}\theta} + \frac{w}{R}\right)\Bigg|^{(i+1)} = 0, \tag{23}$$

with its DQ analogue of

$$\left(\frac{1}{\theta_i}\right)\sum_{m=1}^{N_i} A^{(i)}_{b_i m} u^{(i)}_m + \frac{w^{(i)}_{b_i}}{R_i} - \left(\frac{1}{\theta_{i+1}}\right)\sum_{m=1}^{N_{i+1}} A^{(i+1)}_{b_{i+1} m} u^{(i+1)}_m - \frac{w^{(i+1)}_{b_{i+1}}}{R_{i+1}} = 0. \tag{24}$$

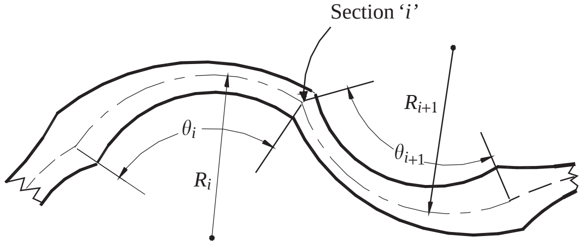


Fig. 2. An arbitrary arch with sudden changes in geometry. The arch is made of sub-circular arches at different sections.

In the above, $N_i$ represents the total number of grid points in sub-domain '$i$', and $b_i$ represents the end grid point in $i$th sub-domain. Due to the fact that the number of grid points in each sub-domain may be unequal, their weighting coefficients are different.

Since the DQ method has solved the strong form of the governing equations, the compatibility conditions in a strong form become a necessity. The continuity of axial forces, bending moments, and shear forces and their respective DQ analogue become as follows:

*Axial force*

$$\frac{AE}{R}\left(\frac{\mathrm{d}w}{\mathrm{d}\theta}-u\right)\bigg|^{(i)}-\frac{AE}{R}\left(\frac{\mathrm{d}w}{\mathrm{d}\theta}-u\right)\bigg|^{(i+1)}=0, \tag{25}$$

$$\frac{A_{b_i}E^{(i)}}{R_i}\left[\frac{1}{\theta_i}\sum_{m=1}^{N_i}A_{b_im}^{(i)}w_m^{(i)}-u_{b_i}^{(i)}\right]-\frac{A_{b_{i+1}}E^{(i+1)}}{R_{i+1}}\left[\frac{1}{\theta_{i+1}}\sum_{m=1}^{N_{i+1}}A_{b_{i+1}m}^{(i+1)}w_m^{(i+1)}-u_{b_{i+1}}^{(i+1)}\right]=0. \tag{26}$$

*Bending moment*

$$\frac{EI}{R^2}\left(\frac{\mathrm{d}^2u}{\mathrm{d}\theta^2}+u\right)\bigg|^{(i)}-\frac{EI}{R^2}\left(\frac{\mathrm{d}^2u}{\mathrm{d}\theta^2}+u\right)\bigg|^{(i+1)}=0, \tag{27}$$

$$\frac{E^{(i)}I_{b_i}}{R_i^2}\left[\frac{1}{\theta_i^2}K_{b_i}^{(i)}+u_{b_i}^{(i)}\right]-\frac{E^{(i+1)}I_{b_{i+1}}}{R_{i+1}^2}\left[\frac{1}{\theta_{i+1}^2}K_{b_{i+1}}^{(i+1)}+u_{b_{i+1}}^{(i+1)}\right]=0. \tag{28}$$

*Shear force*

$$\begin{aligned}&\frac{1}{R^3}\left[EI\left(\frac{\mathrm{d}^3u}{\mathrm{d}\theta^3}+\frac{\mathrm{d}u}{\mathrm{d}\theta}\right)+\frac{\mathrm{d}(EI)}{\mathrm{d}\theta}\left(\frac{\mathrm{d}^2u}{\mathrm{d}\theta^2}+u\right)\right]\bigg|^{(i)}\\&\quad-\frac{1}{R^3}\left[EI\left(\frac{\mathrm{d}^3u}{\mathrm{d}\theta^3}+\frac{\mathrm{d}u}{\mathrm{d}\theta}\right)+\frac{\mathrm{d}(EI)}{\mathrm{d}\theta}\left(\frac{\mathrm{d}^2u}{\mathrm{d}\theta^2}+u\right)\right]\bigg|^{(i+1)}=0,\end{aligned} \tag{29}$$

$$\begin{aligned}&\frac{E^{(i)}}{(R_i\theta_i)^3}\left[I_{b_i}\sum_{n=1}^{N_i}\sum_{m=2}^{N_i-1}A_{b_im}^{(i)}B_{mn}^{(i)}u_n^{(i)}+I_{b_i}A_{b_i1}^{(i)}K_1^{(i)}+I_{b_i}A_{b_iN_i}^{(i)}K_{N_i}^{(i)}+I'_{b_i}K_{b_i}^{(i)}+I_{b_i}\theta_i^2\sum_{m=1}^{N_i}A_{b_im}^{(i)}u_m^{(i)}\right.\\&\left.+I'_{b_i}\theta_i^2u_{b_i}^{(i)}\right]-\frac{E^{(i+1)}}{(R_{i+1}\theta_{i+1})^3}\left[I_{b_{i+1}}\sum_{n=1}^{N_{i+1}}\sum_{m=2}^{N_{i+1}-1}A_{b_{i+1}m}^{(i+1)}B_{mn}^{(i+1)}u_n^{(i+1)}+I_{b_{i+1}}A_{b_{i+1}1}^{(i+1)}K_1^{(i+1)}\right.\\&\left.+I_{b_{i+1}}A_{b_{i+1}N_{i+1}}^{(i+1)}K_{N_{i+1}}^{(i+1)}+I'_{b_{i+1}}K_{b_{i+1}}^{(i+1)}+I_{b_{i+1}}\theta_{i+1}^2\sum_{m=1}^{N_{i+1}}A_{b_{i+1}m}^{(i+1)}u_m^{(i+1)}+I'_{b_{i+1}}\theta_{i+1}^2u_{b_{i+1}}^{(i+1)}\right]=0.\end{aligned} \tag{30}$$

Using the analogues equations Eqs. (24), (26), (28) and (30), in addition to the external boundary conditions, one has an assembled system of equations similar to Eq. (18). The assembled form of the governing equations has a similar form to Eq. (8). Therefore similar to the procedure used for a single domain, the boundary degrees of freedom, i.e., $\{U_b\}$, should be eliminated from the assembled governing equations. The resulting eigenvalue problems should then be solved to obtain the natural frequencies and their related mode shapes.

## 5. Numerical results

All numerical results are based on the extensible theory. The natural frequencies presented in Tables 1–10 are non-dimensionalized. To obtain the results for inextensible arches, in all related examples the value of the slenderness ratio is chosen to be $S_r = 10^4$. Due to the fact that most previous results are based on inextensible theory, most of the examples are chosen with the inextensible assumption to verify the accuracy of the method. The convergence and the stability of the results are proved in Sections 5.1 and 5.2 for some different boundary conditions and geometries for the arches under consideration.

### 5.1. Uniform circular arch

A circular arch with different opening angles and under conditions with at least one edge free (the boundary condition to which DQM is most sensitive) is considered. The convergence and the stability of the evaluated fundamental natural frequencies are shown in Table 1. As shown, well converged results can be obtained with $N = 9$, however results converged to six significant digits can be obtained with $N = 14$. The accuracy of these results is checked by comparing them with those of other numerical methods in Table 2. It is noteworthy to see that the results from the present methodology are very close to those of other techniques such as GDQR [15]. The results are slightly greater than those of the Cell Discretization Method (CDM) which predicts a lower bound to the fundamental frequency [1].

### 5.2. Parabolically variable thickness ring

Gutierrez and Laura [11] have studied the fundamental natural frequency of a completely free and a simply supported ring as shown in Fig. 3. These examples have been considered here and the

Table 1
Convergence and stability of non-dimensional fundamental natural frequencies ($\lambda_i$) for a circular arch under different opening angles and boundary conditions

| Boundary conditions | $\theta_o$ | Number of grid points ($N$) | | | | | |
|---|---|---|---|---|---|---|---|
| | | 9 | 11 | 13 | 14 | 15 | 19 |
| C–F | 10° | 115.456 | 115.496 | 115.496 | 115.496 | 115.496 | 115.496 |
| | 90° | 1.4971 | 1.4982 | 1.4982 | 1.4982 | 1.4982 | 1.4982 |
| | 180° | 0.4291 | 0.4352 | 0.4353 | 0.4352 | 0.4352 | 0.4352 |
| S–F | 10° | 502.857 | 504.036 | 503.988 | 503.989 | 503.989 | 503.989 |
| | 90° | 4.8971 | 4.8866 | 4.8868 | 4.8868 | 4.8868 | 4.8868 |
| | 180° | 0.9400 | 0.9180 | 0.9188 | 0.9188 | 0.9188 | 0.9188 |
| F–F | 10° | 738.543 | 733.441 | 733.652 | 733.649 | 733.649 | 733.649 |
| | 90° | 8.5342 | 8.3851 | 8.3913 | 8.3912 | 8.3912 | 8.3912 |
| | 180° | 1.9643 | 1.8307 | 1.8374 | 1.8372 | 1.8372 | 1.8372 |

Table 2
Non-dimensional fundamental natural frequency ($\lambda_1$) of a uniform circular arch under different boundary conditions

| $\theta_o$ | C–F | | | | S–F | | F–F | |
|---|---|---|---|---|---|---|---|---|
| | Present | GDQ | FEM | CDM | Present | GDQ | Present | GDQ |
| 10° | 115.4953 | 115.4953 | | | 503.9888 | 503.9888 | 733.6490 | 733.6490 |
| 20° | 28.9274 | 28.9274 | 28.920 | 28.196 | 124.4238 | 124.4238 | 182.8018 | 182.8019 |
| 30° | 12.8964 | 12.8964 | | | 54.1996 | 54.1996 | 80.8026 | 80.8026 |
| 40° | 7.2857 | 7.2857 | 7.2827 | 7.1035 | 29.6905 | 29.6905 | 45.1137 | 45.1137 |
| 60° | 3.2784 | 3.2784 | 3.2738 | 3.197 | 12.3434 | 12.3434 | 19.6501 | 19.6501 |
| 80° | 1.8763 | 1.8763 | 1.8766 | 1.8303 | 6.4319 | 6.4319 | 10.7730 | 10.7730 |
| 90° | 1.4982 | 1.4982 | | | 4.8868 | 4.8868 | 8.3912 | 8.3912 |
| 100° | 1.2279 | 1.2279 | 1.2277 | 1.195 | 3.8080 | 3.8080 | 6.6961 | 6.6961 |
| 120° | 0.8762 | 0.8762 | 0.8761 | 0.8544 | 2.4564 | 2.4564 | 4.5088 | 4.5088 |
| 140° | 0.6647 | 0.6647 | 0.6647 | 0.648 | 1.6885 | 1.6885 | 3.2122 | 3.2122 |
| 160° | 0.5282 | 0.5282 | 0.5283 | 0.510 | 1.2202 | 1.2202 | 2.3882 | 2.3882 |
| 180° | 0.4352 | 0.4352 | 0.4355 | 0.4242 | 0.9188 | 0.9188 | 1.8372 | 1.8372 |

Table 3
Non-dimensional fundamental natural frequency ($\lambda_1$) of a parabolically variable thickness ring: (a) simply supported and, (b) completely free ring

| $\alpha$ | Number of grid points | | | | | | | | ORR [11] | CDQ [11] |
|---|---|---|---|---|---|---|---|---|---|---|
| | 5 | 7 | 9 | 11 | 13 | 14 | 15 | 24 | | |
| (a) *Simply supported ring* | | | | | | | | | | |
| 1 | 2.7843 | 2.2670 | 2.2668 | 2.2667 | 2.2667 | 2.2667 | 2.2667 | 2.2667 | 2.274 | 2.268 |
| 1.1 | 2.7953 | 2.4134 | 2.4136 | 2.4136 | 2.4136 | 2.4136 | 2.4136 | 2.4136 | 2.416 | 2.417 |
| 1.2 | 2.7710 | 2.5573 | 2.5567 | 2.5567 | 2.5567 | 2.5567 | 2.5567 | 2.5567 | 2.557 | 2.561 |
| 1.3 | 2.7119 | 2.7021 | 2.6964 | 2.6965 | 2.6965 | 2.6965 | 2.6965 | 2.6965 | 2.697 | 2.701 |
| 1.4 | 2.6169 | 2.8512 | 2.8330 | 2.8334 | 2.8334 | 2.8334 | 2.8334 | 2.8334 | 2.834 | 2.839 |
| 1.5 | 2.4835 | 3.0077 | 2.9668 | 2.9676 | 2.9676 | 2.9676 | 2.9676 | 2.9676 | 2.970 | 2.976 |
| (b) *Completely free ring* | | | | | | | | | | |
| 1 | 2.7344 | 2.6822 | 2.6833 | 2.6833 | 2.6833 | 2.6833 | 2.6833 | 2.6833 | 2.687 | 2.686 |
| 1.1 | 2.8994 | 2.8482 | 2.8451 | 2.8452 | 2.8452 | 2.8452 | 2.8452 | 2.8452 | 2.846 | 2.849 |
| 1.2 | 3.0279 | 3.0182 | 3.0062 | 3.0062 | 3.0062 | 3.0062 | 3.0062 | 3.0062 | 3.006 | 3.010 |
| 1.3 | 3.1271 | 3.1849 | 3.1668 | 3.1665 | 3.1665 | 3.1665 | 3.1665 | 3.1665 | 3.167 | 3.171 |
| 1.4 | 3.2023 | 3.3450 | 3.3270 | 3.3262 | 3.3263 | 3.3263 | 3.3263 | 3.3263 | 3.326 | 3.332 |
| 1.5 | 3.2596 | 3.4948 | 3.4863 | 3.4858 | 3.4858 | 3.4858 | 3.4858 | 3.4858 | 3.486 | 3.493 |

results are shown in Table 3. Also, the results from the optimized Rayleigh–Ritz (ORR) method and conventional DQ (CDQ) methodology as presented by Gutierrez and Laura are shown in this table. For both cases, the ring has a rectangular cross-section with constant width and a parabolic variable thickness according to $h(x) = h_o[-(4/\pi^2)(\alpha - 1)x^2 + (4/\pi)(\alpha - 1)x + 1]$, where $x = \theta/\theta_o$

Table 4
Non-dimensional natural frequencies for an unsymmetric arch under different boundary conditions

| | $\alpha = 0.1$ | | $\alpha = 0.2$ | | $\alpha = 0.3$ | | $\alpha = 0.4$ | |
|---|---|---|---|---|---|---|---|---|
| | Present | GDQR [15] | Present | GDQR [15] | Present | GDQR [15] | Present | GDQR [15] |
| S–S ($\lambda_1$) | | | | | | | | |
| $\theta_o = 10°$ | 1290.485 | 1290.485 | 1281.335 | 1281.336 | 1265.764 | 1265.767 | 1243.234 | 1243.238 |
| 20° | 320.7631 | 320.7631 | 318.4851 | 318.4851 | 314.6083 | 314.6084 | 308.9986 | 308.9987 |
| 40° | 78.3731 | 78.3731 | 77.8126 | 77.8126 | 76.8588 | 76.8588 | 75.4785 | 75.4785 |
| 60° | 33.5461 | 33.5461 | 33.3034 | 33.3034 | 32.8904 | 32.8904 | 32.2929 | 32.2928 |
| 80° | 17.9206 | 17.9206 | 17.7890 | 17.7890 | 17.5649 | 17.5649 | 17.2406 | 17.2406 |
| C–C ($\lambda_1$) | | | | | | | | |
| $\theta_o = 10°$ | 2016.983 | 2016.983 | 2001.812 | 2001.813 | 1975.993 | 1975.996 | 1938.632 | 1938.637 |
| 20° | 502.3033 | 502.3033 | 498.5259 | 498.5260 | 492.0976 | 492.0978 | 482.7954 | 482.7959 |
| 40° | 123.6698 | 123.6698 | 122.7406 | 122.7406 | 121.1591 | 121.1592 | 118.8708 | 118.8708 |
| 60° | 53.6074 | 53.6075 | 53.2053 | 53.2053 | 52.5208 | 52.5209 | 51.5304 | 51.5305 |
| 80° | 29.1456 | 29.1456 | 28.9275 | 28.9275 | 28.5564 | 28.5564 | 28.0193 | 28.0193 |
| C–F ($\lambda_1$) | | | | | | | | |
| $\theta_o = 10°$ | 101.6757 | 101.6757 | 88.4809 | 88.4809 | 75.8416 | 75.8419 | 63.6878 | 63.6881 |
| 20° | 25.4671 | 25.4671 | 22.1631 | 22.1631 | 18.9979 | 18.9980 | 15.9531 | 15.9544 |
| 40° | 6.4152 | 6.4152 | 5.5839 | 5.5839 | 4.7872 | 4.7873 | 4.0207 | 4.0211 |
| 60° | 2.8875 | 2.8875 | 2.5140 | 2.5140 | 2.1560 | 2.1560 | 1.8114 | 1.8116 |
| 80° | 1.6532 | 1.6532 | 1.4399 | 1.4399 | 1.2354 | 1.2354 | 1.0385 | 1.0385 |
| C–F ($\lambda_2$) | | | | | | | | |
| $\theta_o = 10°$ | 692.2050 | 692.2051 | 660.9591 | 660.9595 | 626.7909 | 626.7922 | 589.3152 | 589.2368 |
| 20° | 171.1086 | 171.1086 | 163.2148 | 163.2150 | 154.5999 | 154.6006 | 145.1560 | 145.1512 |
| 40° | 41.0089 | 41.0089 | 38.9736 | 38.9737 | 36.7690 | 36.7692 | 34.3702 | 34.3693 |
| 60° | 17.1390 | 17.1390 | 16.2107 | 16.2108 | 15.2158 | 15.2158 | 14.1445 | 14.1441 |
| 80° | 8.9728 | 8.9728 | 8.4461 | 8.4461 | 7.8878 | 7.8878 | 7.2934 | 7.2932 |
| S–F ($\lambda_1$) | | | | | | | | |
| $\theta_o = 10°$ | 489.2786 | 489.2786 | 472.9768 | 472.9768 | 454.7679 | 454.7681 | 434.2522 | 434.2458 |
| 20° | 120.6608 | 120.6608 | 116.5046 | 116.5046 | 111.8773 | 111.8774 | 106.6801 | 106.6792 |
| 40° | 28.6833 | 28.6833 | 27.5837 | 27.5837 | 26.3735 | 26.3735 | 25.0296 | 25.0296 |
| 60° | 11.8668 | 11.8668 | 11.3540 | 11.3540 | 10.7979 | 10.7979 | 10.1893 | 10.1893 |
| 80° | 6.1535 | 6.1535 | 5.8585 | 5.8585 | 5.5431 | 5.5431 | 5.2029 | 5.2029 |
| S–F ($\lambda_2$) | | | | | | | | |
| $\theta_o = 10°$ | 1622.040 | 1622.047 | 1600.490 | 1600.486 | 1572.893 | 1572.888 | 1538.571 | 1538.576 |
| 20° | 403.7542 | 403.7565 | 398.2833 | 398.2820 | 391.2886 | 391.2870 | 382.5936 | 382.5978 |
| 40° | 99.2894 | 99.2899 | 97.8566 | 97.8563 | 96.0366 | 96.0363 | 93.7826 | 93.7838 |
| 60° | 43.0319 | 43.0322 | 42.3657 | 42.3656 | 41.5270 | 41.5270 | 40.4947 | 40.4953 |
| 80° | 23.4387 | 23.4389 | 23.0517 | 23.0516 | 22.5692 | 22.5692 | 21.9795 | 21.9798 |

and $\alpha$ is the taper parameter. To obtain the fundamental natural frequency, Gutierrez and Laura have modelled one-half and one-quarter of the ring, respectively, for simply supported and the free boundary conditions cases. This is followed here as well, but one should note that for the case

Table 5
The first eight non-dimensional natural frequencies ($\theta_o^2 \lambda_i$) of a simply supported uniform circular arch at different slenderness ratio ($\theta_o = 90°$)

| Method | $S_r$ | Mode sequences | | | | | | | |
|---|---|---|---|---|---|---|---|---|---|
| | | 1 | 2 | 3 | 4 | 5 | 6 | 7 | 8 |
| (a) *Without rotary inertia effect* | | | | | | | | | |
| Present | 11.78 | 18.081 | 29.923 | 45.535 | 71.514 | 89.770 | 110.64 | 148.23 | 155.88 |
| Ref. [3] | | 18.08 | 29.93 | 45.54 | 71.52 | 89.76 | 110.7 | 148.23 | 155.9 |
| Present | 23.56 | 33.320 | 33.560 | 81.481 | 84.892 | 152.43 | 153.78 | 225.72 | 241.66 |
| Ref. [3] | | 33.32 | 33.56 | 81.49 | 84.89 | 152.5 | 153.8 | 225.7 | 241.7 |
| Present | 47.12 | 33.819 | 61.832 | 90.977 | 144.83 | 171.24 | 241.43 | 305.47 | 350.89 |
| Ref. [3] | | 33.82 | 61.84 | 90.98 | 144.8 | 171.2 | 241.5 | 305.5 | 351.8 |
| Present | 117.8 | 33.939 | 78.710 | 151.84 | 174.56 | 247.05 | 345.16 | 414.02 | 479.43 |
| Ref. [3] | | 33.94 | 78.71 | 151.9 | 174.6 | 247.1 | 345.4 | 414.1 | 480.1 |
| Present | 251.3 | 33.956 | 79.719 | 152.11 | 235.26 | 349.19 | 380.16 | 486.28 | 624.09 |
| Ref. [3] | | 33.96 | 79.72 | 152.1 | 235.3 | 349.4 | 380.2 | 486.9 | 625.4 |
| Present | 377.0 | 33.958 | 79.851 | 152.14 | 237.06 | 349.39 | 466.89 | 585.41 | 625.36 |
| Ref. [3] | | 33.96 | 79.85 | 152.2 | 237.1 | 349.7 | 467.5 | 585.6 | 626.8 |
| (b) *Including rotary inertia effect* | | | | | | | | | |
| Present | 23.56 | 32.547 | 33.294 | 79.536 | 80.523 | 136.96 | 150.84 | 203.31 | 223.32 |
| Ref. [4] | | 32.55 | 33.30 | 79.54 | 80.5 | 137.0 | 150.9 | 203.4 | 223.3 |
| Present | 47.12 | 33.601 | 61.587 | 89.549 | 141.77 | 168.88 | 229.84 | 304.24 | 326.64 |
| Ref. [4] | | 33.60 | 61.59 | 89.56 | 141.8 | 168.9 | 229.9 | 304.3 | 326.9 |
| Present | 94.25 | 33.870 | 77.486 | 142.76 | 150.39 | 241.29 | 317.39 | 354.06 | 466.44 |
| Ref. [4] | | 33.87 | 77.49 | 142.8 | 150.4 | 241.4 | 317.4 | 354.3 | 467.1 |
| Present | 188.5 | 33.938 | 79.444 | 151.74 | 229.34 | 295.40 | 347.16 | 478.28 | 610.10 |
| Ref. [4] | | 33.94 | 79.45 | 151.8 | 229.34 | 295.4 | 347.4 | 478.9 | 611.1 |
| Present | 377.0 | 33.955 | 79.831 | 152.06 | 236.86 | 348.97 | 466.21 | 585.20 | 624.09 |
| Ref. [4] | | 33.96 | 79.83 | 152.1 | 236.9 | 349.0 | 466.8 | 585.3 | 625.1 |

of a completely free ring, the boundary conditions in the present formulation become guided supports for both ends. As can be seen in Table 3, accurate solutions can be obtained with only nine grid points for all values of taper parameter $\alpha$. Also, it is interesting to note that the converged fundamental natural frequencies are always slightly less than those of the Rayleigh–Ritz method, which is fruitful, since the former gives an upper bound of fundamental natural frequencies. It is interesting that the $\delta$-technique, employed by Gutierrez and Laura produces

Table 6
The first four non-dimensional natural frequencies ($\theta_o^2 \lambda_i$) for a simply supported unsymmetric circular arch at various slenderness ratios: (a) without rotary inertia effect, (b) including rotary inertia ($\theta_o = 90°$)

| $S_r$ | (a) | | | | (b) | | | |
|---|---|---|---|---|---|---|---|---|
| | Mode sequences | | | | Mode sequences | | | |
| | 1 | 2 | 3 | 4 | 1 | 2 | 3 | 4 |
| $\alpha = 0.2$ | | | | | | | | |
| 10 | 15.7321 | 27.5084 | 41.7016 | 61.9394 | 15.0512 | 26.4509 | 36.6221 | 59.8374 |
| 20 | 28.4944 | 33.0362 | 69.7577 | 83.4926 | 28.1055 | 32.1210 | 68.5767 | 76.6721 |
| 40 | 33.3846 | 54.1716 | 87.5759 | 131.7111 | 33.0889 | 53.9646 | 85.5789 | 130.1944 |
| 100 | 33.5913 | 77.3912 | 148.9517 | 151.8941 | 33.5420 | 77.1428 | 148.2080 | 151.3740 |
| 200 | 33.6177 | 78.8493 | 150.6174 | 229.7436 | 33.6053 | 78.7802 | 150.3466 | 229.1882 |
| 400 | 33.6242 | 79.1319 | 150.7037 | 234.8868 | 33.6211 | 79.1144 | 150.6357 | 234.7231 |
| 500 | 33.6250 | 79.1641 | 150.7135 | 235.1967 | 33.6230 | 79.1528 | 150.6699 | 235.0911 |
| 1000 | 33.6261 | 79.2064 | 150.7264 | 235.5594 | 33.6256 | 79.2036 | 150.7155 | 235.5328 |
| 10 000 | 33.6264 | 79.2202 | 150.7306 | 235.6682 | 33.6264 | 79.2202 | 150.7306 | 235.6682 |
| $\alpha = 0.4$ | | | | | | | | |
| 10 | 15.3808 | 27.2389 | 41.0108 | 61.7392 | 14.6229 | 26.2164 | 36.2061 | 59.1208 |
| 20 | 27.4516 | 33.0317 | 69.2042 | 81.4075 | 26.9219 | 32.2817 | 68.1048 | 74.9140 |
| 40 | 32.2224 | 53.8479 | 85.6098 | 130.0347 | 31.9341 | 53.6324 | 128.3776 | 149.8200 |
| 100 | 32.5317 | 75.2261 | 144.2728 | 151.5037 | 32.4839 | 74.9931 | 143.4350 | 151.1600 |
| 200 | 32.5682 | 76.5783 | 146.0861 | 223.2404 | 32.5562 | 76.5140 | 145.8354 | 222.7171 |
| 400 | 32.5741 | 76.8284 | 146.1292 | 227.5854 | 32.5771 | 76.8448 | 146.1922 | 227.7362 |
| 500 | 32.5782 | 76.8752 | 146.2038 | 228.0233 | 32.5763 | 76.8647 | 146.1634 | 227.9260 |
| 1000 | 32.5796 | 76.9152 | 146.2190 | 228.3621 | 32.5791 | 76.9126 | 146.2089 | 228.3376 |
| 10 000 | 32.5801 | 76.9283 | 146.2239 | 228.4643 | 32.5801 | 76.9283 | 146.2238 | 228.4640 |

results for the tapered ring that are greater than those of the Rayleigh–Ritz method. Excellent rate of convergence and stability of the results for the present method, are other important points.

### 5.3. Unsymmetrical arch under different boundary conditions

An unsymmetric variable section arch, as shown in Fig. 4, is considered here with classical boundary conditions. The results are compared with those of Liu and Wu [15] for the same problem. The arch cross-sectional height varies as $h(x) = h_o[1 + \alpha(2x - 1)]$, where $\alpha$ is a taper parameter. One should note that the height ratio at both ends of the arches is $(1 + \alpha)/(1 - \alpha)$. For example, for the case that $\alpha = 0.4$, this ratio becomes 2.33333, which signifies a sufficiently steep variation. Similarly to Liu and Wu [15], for both ends simply supported or clamped, only the fundamental natural frequencies are to be presented here. For other cases with an edge free, the second natural frequencies are also presented. A wide range of opening angle is considered. Fully converged results with six significant digits are obtained with fifteen grid points. The results are presented in Table 4. Excellent agreement between the solutions of the present algorithm and those of GDQR [15] is achieved.

Table 7
The first four non-dimensional natural frequencies ($\lambda_i$) for an unsymmetric circular arch ($\theta_o = 90°$) for a range of slenderness ratios under two types of boundary conditions

| | $S_r$ | $\alpha = 0.2$ | | | | $\alpha = 0.4$ | | | |
|---|---|---|---|---|---|---|---|---|---|
| | | 1 | 2 | 3 | 4 | 1 | 2 | 3 | 4 |
| (a) C–F | 10 | 1.1459 | 5.2464 | 9.2412 | 19.0111 | 0.8281 | 4.6070 | 8.5326 | 18.6866 |
| | 20 | 1.1492 | 6.1770 | 15.1378 | 23.6891 | 0.8297 | 5.3199 | 14.1893 | 22.5310 |
| | 40 | 1.1500 | 6.3606 | 20.9929 | 32.7188 | 0.8301 | 5.4686 | 19.5914 | 31.2566 |
| | 100 | 1.1503 | 6.4065 | 21.7711 | 45.1050 | 0.8302 | 5.5068 | 20.3880 | 43.0568 |
| | 200 | 1.1503 | 6.4128 | 21.8426 | 45.4646 | 0.8302 | 5.5121 | 20.4636 | 43.4269 |
| | 400 | 1.1503 | 6.4144 | 21.8593 | 45.5306 | 0.8303 | 5.5135 | 20.4813 | 43.4950 |
| | 1000 | 1.1503 | 6.4149 | 21.8614 | 45.5477 | 0.8303 | 5.5138 | 20.4863 | 43.5127 |
| | 4000 | 1.1503 | 6.4149 | 21.8648 | 45.5508 | 0.8303 | 5.5139 | 20.4871 | 43.5158 |
| (b) S–F | 10 | 4.1486 | 8.4542 | 17.3218 | 21.3077 | 3.6562 | 7.9851 | 16.8988 | 20.9266 |
| | 20 | 4.3709 | 15.0103 | 19.7722 | 38.7134 | 3.8593 | 14.0434 | 19.2201 | 37.9870 |
| | 40 | 4.4168 | 17.6033 | 32.6997 | 41.1227 | 3.9032 | 16.6963 | 31.2418 | 39.8390 |
| | 100 | 4.4289 | 17.8385 | 39.4780 | 68.3066 | 3.9150 | 16.9810 | 38.0320 | 65.7725 |
| | 200 | 4.4307 | 17.8642 | 39.6021 | 69.1713 | 3.9167 | 17.0123 | 38.1732 | 66.7949 |
| | 400 | 4.4311 | 17.8704 | 39.6271 | 69.2558 | 3.9171 | 17.0199 | 38.2016 | 66.8930 |
| | 1000 | 4.4312 | 17.8721 | 39.6338 | 69.2758 | 3.9172 | 17.0219 | 38.2091 | 66.9162 |
| | 4000 | 4.4312 | 17.8724 | 39.6350 | 69.2793 | 3.9172 | 17.0223 | 38.2105 | 66.9201 |

### *5.4. A circular arch at different slenderness ratios with and without rotary inertias and under different boundary conditions*

In order to verify the accuracy of the present method for predicting the higher order modes, and also to study the effects of the slenderness ratio and rotary inertia on natural frequencies, a simply supported uniform circular arch is considered again. Twenty grid points are sufficient for results converged to at least five significant digits for the first-eight natural frequencies. The nondimensional natural frequencies are presented in Table 5 with and without considering the rotary inertia effects. The solutions are compared with those of Veletsos et al. [3], and Austin and Veletsos [4]. An excellent agreement is achieved. One can recognize the effects of rotary inertia at higher modes at low $S_r$.

The results for a simply supported unsymmetric variable section circular arch, which include both the effects of slenderness ratio as well as rotary inertia, are presented in Table 6. The cross-sectional height varies as $h(x) = h_o[1 + \alpha(2x - 1)]$. In Table 6 one can also see the effects of inclusion of rotary inertia in calculations of natural frequencies at different values of slenderness ratios. One can see the slenderness ratio has a major effect on the frequencies at higher modes.

Some new results for a variable section, nonsymmetric circular arch with clamped-free and simply-supported free ends are exhibited in Table 7. For all cases in this table, 19 grid points are used to give a solution converged to at least six significant digits. It is interesting to note that for the cases in which one edge is free, the effect of tangential deformation on fundamental natural frequencies becomes negligible. Also, by a comparison of Tables 6 and 7 one can determine the

Table 8
Non-dimensional fundamental frequency ($\lambda_1$) of a uniform circular arch with ends elastically restrained against rotation

| $\theta_o$ | $K_T = 0$ | | | $K_T = 6$ | | | $K_T = 12$ | | |
|---|---|---|---|---|---|---|---|---|---|
| | Present | CDM [1] | Galerkin [1] | Present | CDM [1] | Galerkin [1] | Present | CDM [1] | Galerkin [1] |
| 40° | 78.558 | 78.558 | 78.396 | 90.954 | 90.692 | 91.972 | 98.014 | 97.676 | 100.17 |
| 80° | 17.964 | 17.964 | 17.932 | 22.788 | 22.713 | 23.345 | 24.711 | 24.612 | 25.489 |
| 120° | 6.9268 | 6.9268 | 6.9168 | 9.5407 | 9.5073 | 9.8534 | 10.337 | 10.293 | 10.719 |
| 180° | 2.2667 | 2.2667 | 2.2646 | 3.6196 | 3.6061 | 3.7656 | 3.9151 | 3.8977 | 4.0768 |
| | $K_T = 24$ | | | $K_T = 100$ | | | $K_T = 10^7$ | | |
| | Present | CDM [1] | Galerkin [1] | Present | CDM [1] | Galerkin [1] | Present | CDM [1] | Galerkin [1] |
| 40° | 105.79 | 105.36 | 108.83 | 117.71 | 117.09 | 121.23 | 123.98 | 123.24 | 127.26 |
| 80° | 26.399 | 26.275 | 27.283 | 28.383 | 28.225 | 29.268 | 29.218 | 29.045 | 30.061 |
| 120° | 10.954 | 10.900 | 11.356 | 11.599 | 11.534 | 11.778 | 11.848 | 11.778 | 12.225 |
| 180° | 4.1197 | 4.0991 | 4.2825 | 4.3140 | 4.2903 | 4.4710 | 4.3844 | 4.3595 | 4.5387 |

Table 9
The first 10 non-dimensional natural frequencies ($\lambda_i$) obtained from the approximate theory

| $\theta_o$ | Mode | S–S | | | C–C | | | C–F | | |
|---|---|---|---|---|---|---|---|---|---|---|
| | | Present | Exact [5] | DQ [6] | Present | Exact [5] | DQ [6] | Present | Exact [5] | DQ [6] |
| 40° | 1 | 80.000 | 80.000 | 80.000 | 125.79 | 125.792 | 125.792 | 7.462 | 7.462 | 7.462 |
| | 2 | 172.00 | 172.005 | 172.00 | 226.91 | 226.910 | 226.910 | 44.611 | 44.611 | 44.611 |
| | 3 | 323.00 | 323.000 | 323.00 | 409.20 | 409.204 | 409.204 | 125.845 | 125.845 | 125.845 |
| | 4 | 496.47 | 496.470 | 496.47 | 593.04 | 593.043 | 593.043 | 247.243 | 247.243 | 247.243 |
| | 5 | 982.65 | 982.646 | 728.00 | 854.66 | 854.661 | 854.661 | 409.204 | 409.204 | 409.204 |
| | 6 | 728.00 | 728.000 | 982.65 | 1120.18 | 1120.18 | 1120.18 | 611.678 | 611.678 | 611.678 |
| | 7 | 1295.00 | 1295.00 | 1294.99 | 1462.14 | 1462.14 | 1462.14 | 854.661 | 854.661 | 854.661 |
| | 8 | 1630.74 | 1630.74 | 1630.91 | 1809.02 | 1809.02 | 1809.05 | 1138.15 | 1138.15 | 1138.152 |
| | 9 | 2024.00 | 2024.00 | 2025.80 | 2231.62 | 2231.62 | 2232.19 | 1462.14 | 1462.14 | 1462.115 |
| | 10 | 2440.79 | 2440.80 | 2420.56 | 2659.70 | 2659.73 | 2653.40 | 1826.63 | 1826.63 | 1825.366 |
| 160° | 1 | 4.063 | 4.063 | 4.063 | 7.1898 | 7.189 | 7.1898 | 0.766 | 0.766 | 0.766 |
| | 2 | 9.855 | 9.855 | 9.855 | 13.423 | 13.423 | 13.4234 | 2.315 | 2.315 | 2.315 |
| | 3 | 19.250 | 19.250 | 19.250 | 24.775 | 24.775 | 24.7755 | 7.197 | 7.197 | 7.197 |
| | 4 | 30.107 | 30.107 | 30.107 | 36.239 | 36.239 | 36.2388 | 14.696 | 14.696 | 14.696 |
| | 5 | 44.563 | 44.563 | 44.563 | 52.572 | 52.572 | 52.5723 | 24.775 | 24.775 | 24.775 |
| | 6 | 60.485 | 60.485 | 60.485 | 69.154 | 69.154 | 69.1543 | 37.404 | 37.404 | 37.404 |
| | 7 | 80.000 | 80.000 | 80.000 | 90.517 | 90.517 | 90.517 | 52.572 | 52.572 | 52.572 |
| | 8 | 100.988 | 100.988 | 100.999 | 112.189 | 112.189 | 112.191 | 70.277 | 70.277 | 70.278 |
| | 9 | 125.562 | 125.563 | 125.676 | 138.596 | 138.596 | 138.632 | 90.517 | 90.517 | 90.516 |
| | 10 | 151.615 | 151.615 | 150.345 | 165.345 | 165.348 | 164.952 | 113.290 | 113.290 | 113.210 |

effects of the boundary conditions on the natural frequencies, again, at different values of slenderness ratios.

### 5.5. Elastically restrained uniform circular arch

In order to examine the accuracy of the methodology for non-classical boundary conditions, a circular arch with both ends elastically restrained against rotation (as shown in Fig. 5) is considered. Auciello and De Rosa [1] have used CDM to obtain the fundamental natural frequency of such a circular arch. They have employed the inextensible theory. They have argued their method yields a lower bound for the fundamental natural frequency. Here, the same problem is examined under a wide range of rotational stiffnesses $K_T$ $(= k_t R/EI_o)$ and opening angles. At both ends the torsional stiffness is chosen to be equal. The results are shown in Table 8. For all cases, the results of present analysis are slightly greater than those of CDM but slightly less than those of the Galerkin method [1]. It should be noted here, that in general, the Galerkin method would not result in upper bound values for natural frequencies.

### 5.6. Analysis of uniform circular arch under "approximate theory" assumption

The accuracy of the present method for solving the governing equation of 'approximate theory' is demonstrated through the solutions for nondimensionalized natural frequencies of a uniform

Table 10
Non-dimensional natural frequencies for a symmetric tapered arch under different boundary conditions and with different opening angles

| | $\alpha = 0.1$ | | $\alpha = 0.2$ | | $\alpha = 0.3$ | |
|---|---|---|---|---|---|---|
| | Present | GDQR [15] | Present | GDQR [15] | Present | GDQR [15] |
| C–C ($\lambda_1$) | | | | | | |
| $\theta_o = 10°$ | 2149.7594 | 2149.7593 | 2275.3958 | 2275.3957 | 2399.1619 | 2399.1619 |
| 20° | 535.4500 | 535.4500 | 566.8193 | 566.8193 | 597.7229 | 597.7229 |
| 30° | 236.5183 | 236.5183 | 250.3404 | 250.3404 | 264.1372 | 264.1371 |
| 40° | 131.9088 | 131.9088 | 139.7107 | 139.7107 | 147.3984 | 147.3984 |
| 50° | 83.5073 | 83.5073 | 88.4809 | 88.4809 | 93.3824 | 93.3824 |
| C–C ($\lambda_2$) | | | | | | |
| $\theta_o = 10°$ | 3858.7878 | 3859.2373 | 4073.3759 | 4073.8708 | 4285.6463 | 4286.188 |
| 20° | 963.4028 | 963.4309 | 1017.0119 | 1017.0424 | 1070.0422 | 1070.0756 |
| 30° | 427.1678 | 427.1733 | 450.9602 | 450.9661 | 474.4959 | 474.5023 |
| 40° | 239.4849 | 239.4866 | 252.8411 | 252.8428 | 266.0533 | 266.0552 |
| 50° | 152.6174 | 152.6181 | 161.1432 | 161.1439 | 169.5771 | 169.5779 |
| S–S ($\lambda_1$) | | | | | | |
| $\theta_o = 10°$ | 1357.2106 | 1357.2106 | 1419.0535 | 1419.0535 | 1479.2608 | 1479.2608 |
| 20° | 337.8891 | 337.8891 | 352.7986 | 352.7986 | 367.8006 | 367.8006 |
| 30° | 148.5490 | 148.5490 | 155.3598 | 155.3598 | 161.9904 | 161.9904 |
| 40° | 82.4735 | 82.4735 | 86.2745 | 86.2745 | 89.9750 | 89.9750 |
| 50° | 51.9099 | 51.9095 | 54.3172 | 54.3172 | 56.6613 | 56.6613 |
| S–S ($\lambda_2$) | | | | | | |
| $\theta_o = 10°$ | 2913.1934 | 2913.2945 | 3058.8290 | 3058.9326 | 3202.7096 | 3202.8152 |
| 20° | 726.8991 | 726.9054 | 763.2511 | 763.2575 | 799.1647 | 799.1712 |
| 30° | 322.0205 | 322.0217 | 338.1346 | 338.1359 | 354.0541 | 354.0553 |
| 40° | 180.3159 | 180.3163 | 189.3468 | 189.3472 | 198.2685 | 198.2689 |
| 50° | 114.7310 | 114.7310 | 120.4834 | 120.4836 | 126.1649 | 126.1664 |

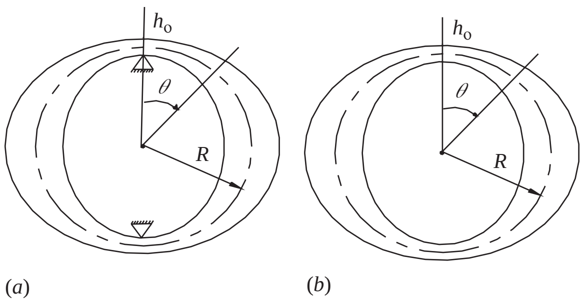


Fig. 3. Ring with a parabolic variable thickness: (a) simply supported, (b) completely free ring.

circular arch under different opening angles and under different boundary conditions as presented in Table 9. These results for the first ten natural frequencies are compared with the exact solutions [5] as well as another DQ solution [6]. Thirty grid points were employed to obtain results

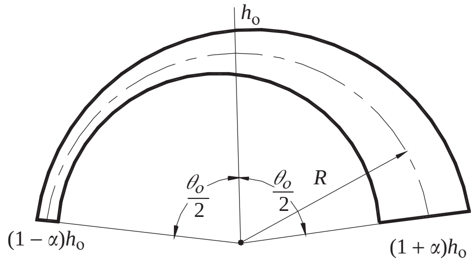


Fig. 4. Unsymmetric arch.

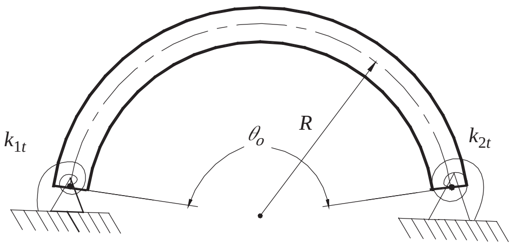


Fig. 5. Arch with ends elastically restrained against rotation.

converged to five significant digits. Excellent agreements are achieved in comparison with the exact solutions both for shallow and deep arches.

### 5.7. Symmetric tapered and unsymmetric stepped arches

To assess, and to demonstrate implementation of the domain decomposition scheme in conjunction with the present DQ methodology for the problems having sudden changes in geometrical cross-section, two examples are considered. In the first example, a symmetric tapered arch, as shown in Fig. 6, under different tapered angle, under two different boundary condition types and at different values for the opening angle is considered. The cross-sectional height varies as

$$h(x) = \begin{cases} h_o[1-\alpha(2x-1)], & \text{when } 0 \leqslant x \leqslant 1/2, \\ h_o[1+\alpha(2x-1)], & \text{when } 1/2 \leqslant x \leqslant 1. \end{cases}$$

This problem has also been studied by Liu and Wu [15] who solved it by GDQR. The results for the first two natural frequencies, using $N = 14$, are shown in Table 10 and compared with those of Liu and Wu [15].

In another example, a stepped circular arch, as shown in Fig. 7, with $h_2/h_1 = 1.25$ is considered. The results of Liu and Wu [15] and Tong et al. [2] are also cited for comparison in Table 11. For the analysis at each sub-domain 14 grid points are used. Excellent agreements are achieved among the different solution procedures.

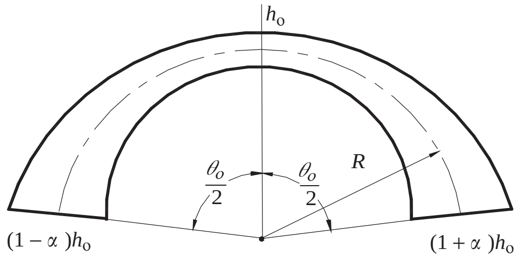


Fig. 6. Symmetric tapered arch.

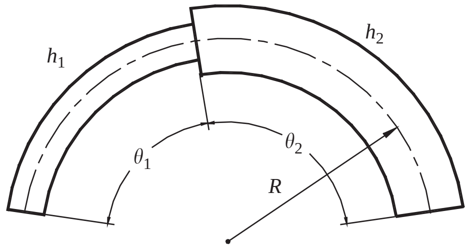


Fig. 7. Unsymmetric stepped arch.

## 6. Conclusions

A general and a computationally efficient DQ solution method for in-plane free vibration analysis of variable section circular arches was presented. In an improvement to the analysis of circular arches, the inextensibility condition assumption was removed. Circular arches under different types of classical boundary conditions, and also with edges elastically restrained against rotation, were examined for shallow as well as deep arches. The DQ solution to the governing equations under "approximate theory" was also developed and examined. The domain decomposition technique in conjunction with DQM was also incorporated for arches with change in their geometry or material properties. The effects of slenderness ratio and the rotary inertia on the solutions were also examined. Employing the algorithm, different examples were analyzed to verify the accuracy and applicability of the methodology. It can be concluded that the present methodology can also be used as an alternative and efficient tool for the solution to similar problems in solid mechanics analysis.

## Appendix A. Evaluation of weighting coefficients

According to DQM, the $m$th order derivative of a field variable $u(x,t)$ with respect to $x$ at an arbitrary point $x_i$ is approximated by

$$\left.\frac{\partial^m u}{\partial x^m}\right|_{x_i} = \sum_{j=1}^{N} A_{ij}^{(m)} u(x_j, t), \tag{A.1}$$

Table 11
Non-dimensional natural frequencies ($\lambda_i$) for an unsymmetric stepped arch under different boundary conditions and with different opening angles

| | Mode sequences | | | | | | | |
|---|---|---|---|---|---|---|---|---|
| | 1 | | | 2 | | 3 | 4 | 5 |
| | Present | GDQR [15] | Ref. [2] | Present | GDQR [15] | Present | Present | Present |
| (a) S–S | | | | | | | | |
| $\theta_o = 10°$ | 1458.837 | 1458.838 | 1458.852 | 3054.560 | 3054.689 | 5823.40 | 8791.24 | 13077.04 |
| 20° | 362.6133 | 362.6133 | 362.609 | 762.165 | 762.173 | 1453.76 | 2196.48 | 3267.18 |
| 30° | 159.6269 | 159.6269 | 159.625 | 337.6350 | 337.6366 | 644.576 | 975.096 | 1450.54 |
| 40° | 88.6024 | 88.6024 | 88.601 | 189.0526 | 189.0531 | 361.376 | 547.605 | 814.736 |
| 50° | 55.7503 | 55.7503 | 55.750 | 120.2845 | 120.2847 | 230.310 | 349.738 | 520.460 |
| 60° | 37.9269 | 37.9269 | 37.926 | 82.9337 | 82.9338 | 159.128 | 242.256 | 360.620 |
| 70° | 27.2019 | 27.2019 | | 60.4173 | 60.4173 | 116.222 | 177.451 | 264.255 |
| 80° | 20.2622 | 20.2622 | | 45.8081 | 45.8082 | 88.3879 | 135.392 | 201.723 |
| (b) C–S | | | | | | | | |
| $\theta_o = 10°$ | 1853.704 | 1853.704 | 1853.663 | 3538.327 | 3538.337 | 6563.38 | 9624.97 | 14165.8 |
| 20° | 461.3518 | 461.3518 | 461.342 | 883.072 | 883.07 | 1638.56 | 2405.02 | 3539.12 |
| 30° | 203.5249 | 203.5249 | 203.520 | 391.3581 | 391.3579 | 726.571 | 1067.74 | 1571.23 |
| 40° | 113.3039 | 113.3039 | 113.014 | 219.2632 | 219.2635 | 407.389 | 599.679 | 882.482 |
| 50° | 71.5644 | 71.5644 | 71.563 | 139.6135 | 139.6136 | 259.671 | 383.033 | 563.709 |
| 60° | 48.9112 | 48.9112 | 48.910 | 96.3523 | 96.3524 | 179.447 | 265.351 | 390.565 |
| 70° | 35.2721 | 35.2721 | | 70.2727 | 70.2727 | 131.091 | 194.396 | 286.182 |
| 80° | 26.4394 | 26.4394 | | 53.3516 | 53.3515 | 99.7225 | 148.346 | 218.445 |
| (c) C–C | | | | | | | | |
| $\theta_o = 10°$ | 2277.434 | 2277.436 | 2277.412 | 4027.230 | 4027.767 | 7366.079 | 10494.09 | 15339.85 |
| 20° | 567.1737 | 567.1738 | 567.170 | 1005.440 | 1005.474 | 1839.008 | 2622.562 | 3832.345 |
| 30° | 250.4748 | 250.4748 | 250.472 | 445.7867 | 445.7933 | 815.4926 | 1164.457 | 1701.336 |
| 40° | 139.6489 | 139.6489 | 139.647 | 249.9069 | 249.909 | 457.2812 | 654.0919 | 955.5034 |
| 50° | 88.3724 | 88.3724 | 88.372 | 159.2458 | 159.2467 | 291.5007 | 417.8631 | 610.3108 |
| 60° | 60.5389 | 60.5389 | 60.538 | 110.0019 | 110.0024 | 201.4672 | 289.5425 | 422.8204 |
| 70° | 43.7766 | 43.7766 | | 80.3138 | 80.3141 | 161.9572 | 212.1714 | 309.7906 |
| 80° | 32.9173 | 32.9173 | | 61.0496 | 61.0498 | 127.5332 | 161.9572 | 236.4499 |

where $A_{ij}^{(m)}$ are the weighting coefficients associated with the $m$th order derivative and $N$ is the number of grid points in the $x$ direction. The weighting coefficients of the first order derivatives are determined according to [7]

$$A_{ij}^{(1)} = \begin{cases} \dfrac{M^{(1)}(x_i)}{(x_i - x_j)M^{(1)}(x_j)} & \text{for } i \neq j, \\ -\sum_{\substack{j=1 \\ i \neq j}}^{N} A_{ij}^{(1)} & \text{for } i = j; \;\; i,j = 1, 2, \ldots, N, \end{cases} \tag{A.2}$$

where $M(x)$ is defined as

$$M(x) = \prod_{j=1}^{N} (x - x_j). \tag{A.3}$$

$M^{(1)}(x)$ is the first order derivative of the function, $M(x)$:

$$M^{(1)}(x_i) = \prod_{j=1,\, j\neq i}^{N} (x_i - x_j). \tag{A.4}$$

In order to evaluate the weighting coefficients of higher order derivatives, recurrence relations may be employed,

$$A_{ij}^{(r)} = \begin{cases} r\left[A_{ii}^{(r-1)}A_{ij}^{(1)} - \dfrac{A_{ij}^{(r-1)}}{x_i - x_j}\right], & i\neq j, \\ -\sum_{\substack{j=1 \\ i\neq j}}^{N} A_{ij}^{(1)}, & i=j; \text{ for } i,j = 1,2,\ldots,N \text{ and } r = 2,3,\ldots,N-1. \end{cases} \tag{A.5}$$

For simplicity, we use the notations

$$A_{ij} = A_{ij}^{(1)}, \quad B_{ij} = A_{ij}^{(2)}. \tag{A.6}$$

In this paper the grid points are located at the so-called Gauss–Lobatto–Chebyshev points,

$$x_i = \frac{1}{2}\left[1 - \cos\left[\frac{(i-1)\pi}{(N-1)}\right]\right]. \tag{A.7}$$

## References


[1] N.M. Auciello, M.A. De Rosa, Free vibration of circular arches: a review, *Journal of Sound and Vibration* 176 (1994) 433–458.

[2] X. Tong, N. Mrad, B. Tabarrok, In-plane vibration of circular arches with variable cross section, *Journal of Sound and Vibration* 212 (1998) 121–140.

[3] A.S. Veletsos, W.J. Austin, C.A.L. Pereira, S.J. Wung, Free in-plane vibration of circular arches, *Journal of Engineering Mechanics* 98 (1972) 311–329.

[4] W.J. Austin, A.S. Veletsos, Free vibration of arches flexible in shear, *Journal of Engineering Mechanics* 99 (1973) 735–753.

[5] J. Henrych, *The Dynamics of Arches and Frames*, Elsevier, Amsterdam, 1981.

[6] M.A. De Rosa, C. Franciosi, Exact and approximate dynamic analysis of circular arches using DQM, *International Journal of Solids and Structures* 37 (2000) 1103–1117.

[7] C.W. Bert, M. Malik, The differential quadrature method in computational mechanics: a review, *Applied Mechanics Reviews* 49 (1996) 1–27.

[8] G. Karami, P. Malekzadeh, A new differential quadrature methodology for beam analysis and the associated DQEM, *Computer Methods in Applied Mechanics and Engineering* 191 (2002) 3509–3526.

[9] G. Karami, P. Malekzadeh, Application of a new differential quadrature methodology for free vibration analysis of plates, *International Journal for Numerical Methods in Engineering* 56 (2003) 847–868.

[10] G. Karami, P. Malekzadeh, An efficient differential quadrature methodology for free vibration analysis of arbitrary straight-sided quadrilateral thin plates, *Journal of Sound and Vibration* 263 (2) (2003) 415–442.

[11] R.H. Gutierrez, P.A.A. Laura, Vibrations of non-uniform rings studied by means of the differential quadrature method, *Journal of Sound and Vibration* 185 (1995) 507–513.
[12] K. Kang, C.W. Bert, A.G. Striz, Vibration and buckling analysis of circular arches using DQM, *Computers and Structures* 60 (1996) 49–57.
[13] K. Kang, C.W. Bert, A.G. Striz, Vibration analysis of horizontally curved beams with warping using DQM, *Journal of Structural Engineering* 122 (1996) 657–662.
[14] K. Kang, C.W. Bert, A.G. Striz, Vibration analysis of shear deformable circular arches by the differential quadrature method, *Journal of Sound and Vibration* 181 (1995) 353–360.
[15] G.R. Liu, T.Y. Wu, In-plane vibration analysis of circular arches by the generalized differential quadrature method, *International Journal of Mechanical Science* 43 (2001) 2597–2611.
[16] K.M. Liew, F.-L. Liu, Differential quadrature method for vibration analysis of shear deformable annular sector plates, *Journal of Sound and Vibration* 230 (2000) 335–356.
[17] M. Liew, K. Han, J.-B.M. Xiao, Differential quadrature method for thick symmetric cross-ply laminates with first-order shears flexibility, *International Journal of Solids and Structures* 33 (1996) 2647–2658.
[18] H. Du, K.M. Liew, M.K. Lim, Generalized differential quadrature method for buckling analysis, *ASCE Journal of Engineering Mechanics* 122 (1996) 95–100.